Chapter 1

Electron Diffraction

Mohsen Asadi Asadabad and Mohammad Jafari Eskandari

Additional information is available at the end of the chapter

http://dx.doi.org/10.5772/61781

Abstract

Electron microscopes are usually supplied with equipment for obtaining diffraction patterns and micrographs from the same area of a specimen and the best results are attained if the complete use is to be made of these combined facilities. Electron diffraction patterns are used to obtain quantitative data including phase identification, orientation relationship and crystal defects in materials, etc. At first, a general introduction including a geometrical and quantitative approach to electron diffraction from a crystalline specimen, the reciprocal lattice and electron diffraction in the electron microscope are presented. The scattering process by an individual atom as well as a crystal, the Bragg law, Laue conditions and structure factor are also discussed. Types of diffraction patterns such as ring pattern, spot pattern and Kikuchi pattern, and general and unique indexing diffraction patterns are explained. The procedure for indexing simple, complicated and imperfect patterns as well as Kikuchi lines and a combination of Kikuchi lines and spots is outlined. The known and unknown materials are identified by indexing patterns. Practical comparisons between various methods of analysing diffraction patterns are also described. The basic diffraction patterns and the fine structure in the patterns including specimen tilting experiments, orientation relationship determination, phase identification, twinning, second phases, crystallographic information, dislocation, preferred orientation and texture, extra spots and streaks are described in detail. Finally, electron diffraction patterns of new materials are investigated.

Keywords: Electron diffraction pattern, Spot and ring pattern, Kikuchi line, Phase identification

1. General introduction

In quantum mechanics, electrons may be considered as particles or waves. Electrons are used in transmission electron microscopy (TEM) because the wavelength of electrons is shorter than the visible light. For this reason, high magnifications can be achieved in TEM. In TEM, tungsten filament is usually used to produce a monochromatic beam of electrons by thermionic or field

emission processes. Electrons are accelerated by applied voltage and focused by the objective lens. These particles with negative charge travel the spiral path when passing through the electromagnetic lenses. Then, this beam of electrons is transmitted through very thin specimen (thickness about 100–300 nm) and magnified by the electromagnetic lens, forming the electron diffraction pattern. Electrons are accelerated to close to the speed of light at high voltages. So, relativistic effects should be considered in equations of electron beam wavelength in electron microscopy at high accelerated voltage. The modified relativistic wavelength is

$$\lambda = \frac{h}{\left(2m_e Ve\left(1 + eV / 2m_e c^2\right)\right)^{1/2}} \tag{1}$$

where h is Planck's constant, m_e is the rest mass of electrons, e is charge of electrons, V is accelerated voltage of electrons and c is the velocity of light. In fact, electron diffraction directly demonstrates the reciprocal lattice of the crystalline lattice of the selected area from a sample [1].

1.1. Elastic scattering of electrons by individual atom

When a beam of electrons transmits through a thin specimen, different interactions can occur such as ionization, secondary emission and excitation with loss of energy and can be scattered by nuclei and electron cloud without loss of energy. The elastic scattering process by an isolated atom is illustrated in Figure 1.Some of the electrons are backscattered and the rest are scattered by nucleus and electron cloud (Rutherford scattering). The atomic scattering amplitude for electrons f_θ (atomic diffraction factor: a measure of the diffracting capability of an isolated atom) is given by

$$f_\theta = \frac{m_e e^2}{2h^2}\left(\frac{\lambda}{sin\theta}\right)^2 \left(Z - f_x\right) \tag{2}$$

where θ is the scattering angle, Z is the atomic number of isolated atom (Rutherford scattering) and f_x is the atomic scattering factor for X-rays. The elastically scattered electrons' main contribution is in the form of diffraction patterns. Most of the particles are scattered within ±5° of the direct incident beam [2].

1.2. Scattering by an ideal crystal structure

For understanding the essence of electron diffraction by a three-dimensional crystal structure of a material, the principles of diffraction of a monochromatic light by Young's double slit experiment should be investigated. First of all, diffraction by two slits is investigated, then, diffraction is generalized to an infinite number of slits and, finally, diffraction from a regular arrangement of atoms is investigated. In Figure 2, the plane waves collide with a barrier with

http://dx.doi.org/10.5772/61781

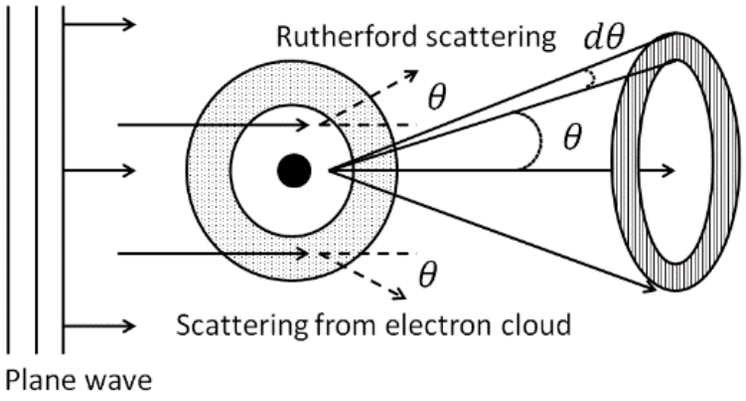

Figure 1. Electrons are as plane wave and black circle is an isolated atom. Electrons are scattered from electron cloud and nucleus of a single atom at the angle θ.

two slits in which the length and width of slits are l and a, respectively, with respect to $l \gg a$. Also, bright and dark fringes are formed on the screen which is placed at a distance S, with respect to $S \gg a$. If the waves are in-phase when passing through the slits, there is relative phase difference between two secondary sources. Two beams of electrons have constructive interference if their relative phase difference is an integer multiple of λ ($\delta = n\lambda$), then the bright fringes are formed on the screen. Similarly, two beams of electrons have unconstructive interference if their relative phase difference is not an integer multiple of λ ($\delta = n\lambda/2$). Therefore, dark fringes are formed on the screen, in which intensity is very low or zero. Alternating bright and dark lines are formed on the screen. The intensity of the bright fringes at the center is very high and away from the center as θ increases, their intensity and width are decreased. In a real three-dimensional crystal lattice, diffraction of electron beams occurs by regular spacing between atoms, which creates an interference pattern.

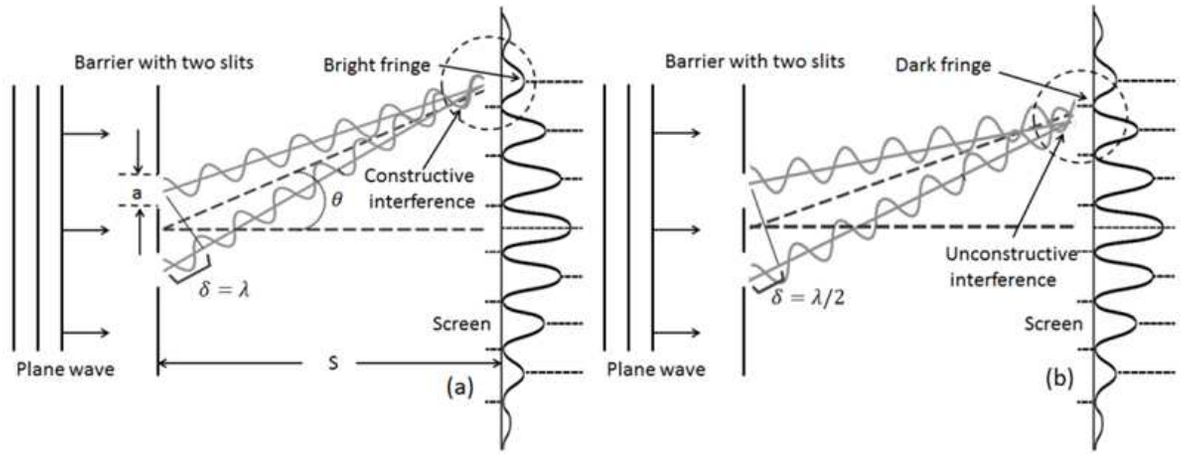

Figure 2. Diffracted beam of electrons by barrier with two slits (Young's slits). (a) Lines bright (constructive interference), (b) Lines dark (unconstructive interference).

In general, electron diffraction is according to kinematical theory and some assumptions must also be considered [2, 3].

1.3. The Bragg law

For studying the scattered and transmitted beams, a cross-section of a thin specimen with a perfect crystal lattice is considered. Incident coherent electron and in-phase beams are radiated from the top surface of the thin specimen. This electron beam is collided with two atoms, each of which belongs to a plane (two adjacent planes) with different *hkl* (Miller indices) with interplanar spacing of crystal lattice being equal to d. Then, the electron beam is diffracted by elastic scattering. These waves are coherent and in-phase after passing through the sample if the path difference of the electron beam is an integer number of wavelength (constructive interference), that is, geometric relationships $AC + AD = n\lambda$ and $AC = AD = dsin\theta$ are satisfied, as can be seen in Figure 3. So, the following relationship is established:

$$2d_{(hkl)}sin\theta = n\lambda \tag{3}$$

where d is the interplanar spacing, θ is the angle between incident and diffracted beams, λ is the electron wavelength and n is the integer number of order diffraction. This relationship is known as the Bragg law. Basically, first-order diffraction is $n=1$ and Miller indices are used for higher orders $n \geq 2$.

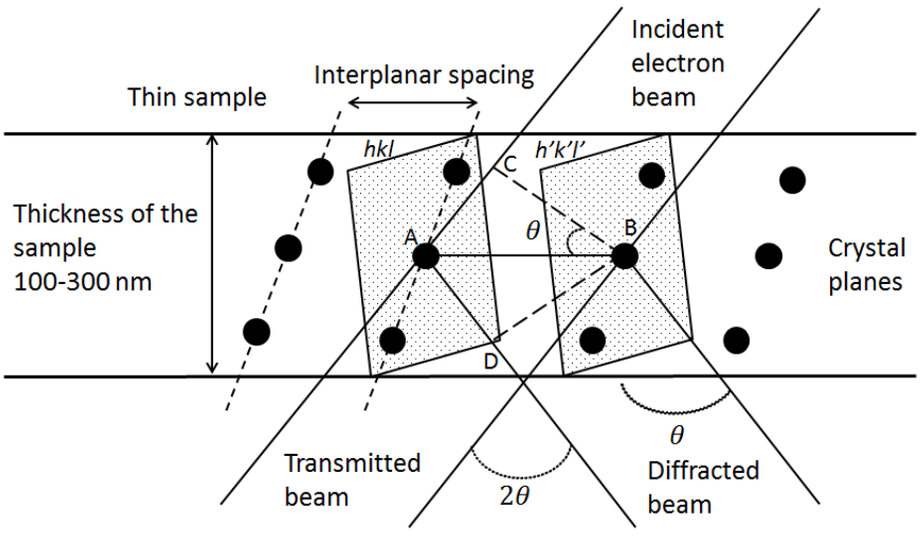

Figure 3. Incident, transmitted and diffracted electron beams in a thin specimen for the Bragg law.

In the Bragg law, electrons are collided with the crystal planes. Some of them are diffracted and the rest are transmitted through the specimen, which does not participate in the formation of the diffraction pattern [1–3].

1.4. The Laue conditions

Diffraction can be considered as a total scattering of individual atoms. So, diffraction is mathematically expressed in terms of total scattering of atoms. The distance from atom A to atom B is described by vector r in three-dimensional space. Also, incident and diffracted beams are described by unit vectors $\boldsymbol{p_0}$ and p, respectively. With the use of these vector notations, we can write paths difference in vector notation as $AC = r.p_0$ and $AD = r.p$. According to the vector relationship in Figure 4, the path difference of wave should be an integer multiple of wavelength and we may write as

$$CAD = \boldsymbol{r}.\boldsymbol{P} = n\lambda \tag{4}$$

The vector $\boldsymbol{r}$, defined in spherical coordinates, is a converted form of vector components x, y and z in Cartesian coordinates, and $\boldsymbol{a}$, $\boldsymbol{b}$ and $\boldsymbol{c}$ are unit vectors defined in the direction of coordinates axes which can be considered as distances between atoms. So, we may write Equation (4) as

$$\begin{aligned} \boldsymbol{P}.\boldsymbol{a} &= h\lambda \\ \boldsymbol{P}.\boldsymbol{b} &= k\lambda \\ \boldsymbol{P}.\boldsymbol{c} &= l\lambda \end{aligned} \tag{5}$$

These algebraic relations are known as Laue conditions. These relations must be satisfied when strong diffraction occurs [2, 3].

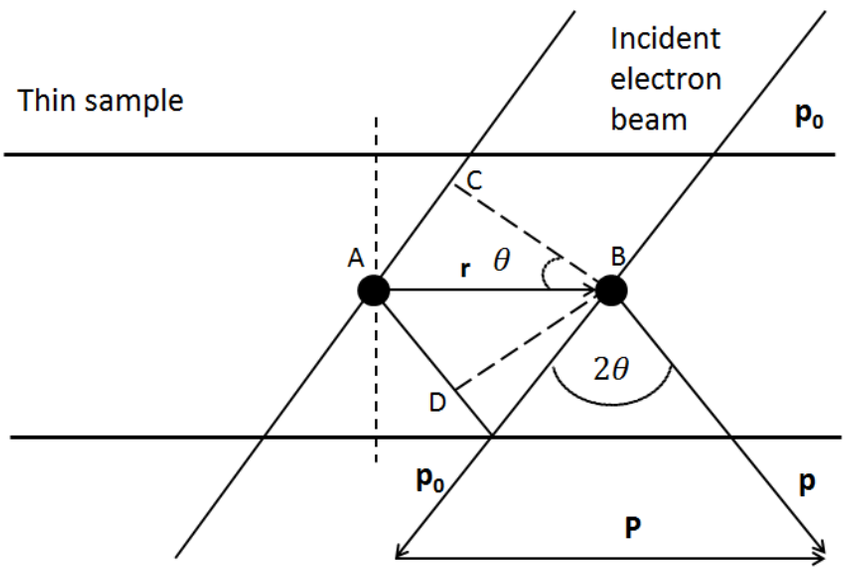

Figure 4. Incident and diffracted waves of atoms in the thin specimen are $\boldsymbol{p_0}$ and p, respectively, the angle between them is 2θ and the distance from atom A to atom B is described by vector r.

1.5. The structure factor

Diffraction intensity is different for each of the crystalline planes because the distribution of atoms per unit area is not the same for individual planes. Using the kinematical theory of electron diffraction, a set of crystal planes can be determined for which the diffraction intensity is zero. The structure factor can be defined as a mathematical function stating the amplitude and phase of electron beam diffracted from crystallographic planes. In the structure factor, the location of atoms in the reflection plane and atomic specifications is considered to describe the diffraction process. Also, the structure factor is the sum of the scattered amplitudes of single atoms f_n and the sum of the phase differences, that is,

$$F_{hkl} = \sum_n f_n exp\left\{2\pi i\left(hx_n + ky_n + lz_n\right)\right\} \tag{6}$$

where x_n, y_n, z_n are positions of the atom in the Cartesian coordinates. The intensity of the diffracted wave is

$$I \propto \left|F\right|^2 \propto f^2\left[1 + cos\left(\pi\left(h+k+l\right)\right)\right]^2 + f^2\left[sin\left(2\pi\left(h+k+l\right)\right)\right]^2 \tag{7}$$

In the above relationship, the intensity is sometimes zero, which belongs to any diffraction not existing in these planes and is called a forbidden reflection. By use of the Bragg law and structure factor, diffracted planes in the crystal can be determined. For intermetallic compounds, the diffraction intensity is different because atomic scattering factors of individual metals forming the intermetallic compound are not the same. For example, intermetallic compounds with an AB structure have diffracted intensity according to the following relations:

$$\begin{aligned} I &\propto \left(f_A + f_B\right)^2 \text{ when } h+k+l \text{ is even} \\ I &\propto \left(f_A - f_B\right)^2 \text{ when } h+k+l \text{ is odd} \end{aligned} \tag{8}$$

Diffraction rules for some of the conventional crystalline structures are presented in Table 1 [2].

Crystal structure	Reflection absent if
simple cubic	all present
f.c.c	*h*, *k*, *l*, mixed odd and even
b.c.c	*h*, *k*, *l* odd
c.p.h	$h+2k=3n$ and *l* is odd
b.c.t	$h+k+l$ odd
Zinc blende	*h*, *k*, *l*, mixed odd and even
Sodium chloride	*h*, *k*, *l*, mixed odd and even
diamond	*h*, *k*, *l*, all even and $h+k+l$ not divisible by four, or *h*, *k*, *l* mixed odd and even

Table 1. Diffraction rules for conventional crystalline structures

1.6. The reciprocal lattice

The reciprocal lattice is an array of points in which each point corresponds to a special plane in the crystal lattice. In fact, each of the planes in real crystal lattice is represented by a point in the reciprocal lattice located at distance $1/d_{hkl}$ from the center O. The distance of a point in the reciprocal lattice to the center is illustrated by the vector $g_{(hkl)}$, which is called the diffraction vector. Diffraction pattern and reciprocal lattice are related to each other and this relation is used for the interpretation of different diffraction patterns. The reciprocal lattice has two special properties:

a. The diffraction vector $g_{(hkl)}$ of reciprocal lattice is perpendicular to the plane of the crystal lattice

b. $g_{(hkl)}=1/d_{hkl}$

The Ewald sphere displays the relation between the reciprocal lattice and the diffraction pattern with a radius of $1/\lambda$. The formation of the Ewald sphere in the reciprocal lattice and the diffraction pattern are depicted in Figure 5. Also, the algebraic relations between incident, transmitted and diffracted beams are shown in this figure. The incident beam of electrons is collided with the thin specimen and then, a certain percentage of the incident beam is transmitted and the rest is diffracted. Using Figure 5, the geometrical relations for distances and angle may be determined from the relation

$$tg2\theta = R/L \tag{9}$$

where θ is the angle between transmitted and diffracted beams, R is the distance between collision points of transmitted and diffracted beams with the screen and L is the distance between the specimen and the screen (the effective camera length). Using the Bragg law and with the assumption of a small θ, relation (9) can be written as follows

$$Rd_{hkl} = L\lambda \tag{10}$$

where $L\lambda$ is a camera constant. The effective camera length and wavelength of the electron are constant and depend on the characterization of transmission electron microscopy [2, 3].

2. Types of electron diffraction patterns

Electron diffraction patterns give crystallographic information about a material and determine different types of materials which can be amorphous, single crystalline or polycrystalline. There are three types of electron diffraction patterns and the formation of each pattern depends on the different conditions of the specimen such as thickness, crystal structure and so on.

1. The polycrystalline materials exhibit ring pattern

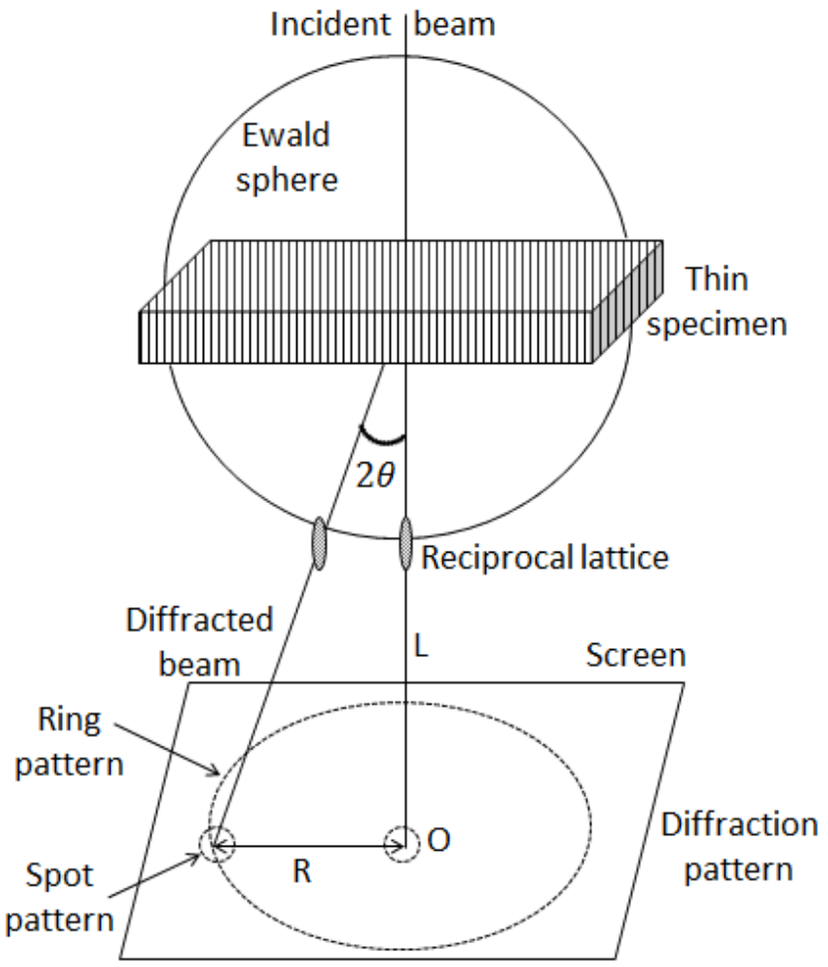

Figure 5. The Ewald sphere is drown in reciprocal lattice. The formation of a diffraction pattern is shown geometrically. The relations between incident, transmitted and diffracted beams, the Ewald sphere and different diffraction patterns are illustrated.

2. The single crystalline materials show (a) spot pattern or (b) Kikuchi line pattern or (c) a combination of spot and Kikuchi line patterns

The spot and Kikuchi line patterns are obtained from a special area of specimen which is called the 'selected area' [5–8]. Selected area electron diffraction (SAED) is a technique in TEM to obtain diffraction patterns that result from the electron beam scattered by the sample lattice.

2.1. Ring pattern

These patterns are created by ultrafine grains of polycrystalline materials. Basically, phases in various polycrystalline materials are determined by interpretation of their ring patterns. For this purpose, we must use a reference specimen for identification of phases as well as specifying interplanar spacing and Miller indices of crystalline planes. Polycrystalline specimens such as pure gold (Au, f.c.c crystal structure with lattice parameter a=4.07 $\mathring{A}$) or pure aluminum (Al, f.c.c crystal structure with lattice parameter a=4.04 $\mathring{A}$) as reference specimens are used to index diffraction patterns of various materials and specify the camera length. To obtain a reference

specimen with a ring diffraction pattern, at first, a copper grid with amorphous carbon coating is provided. Then, by use of a sputter coating device, a thin layer of pure gold with a thickness of about 20 nm is coated on the grid. Finally, the diffraction pattern of the specimen is taken which is in a ring shape and continuous, as can be seen in Figure 6. The planes of the gold specimen are specified by Miller indices. The pure gold sample is known as standard sample and is used for identification of crystalline planes and measurement of interplanar spacing of unknown materials with ring patterns and determination of phases in alloys.

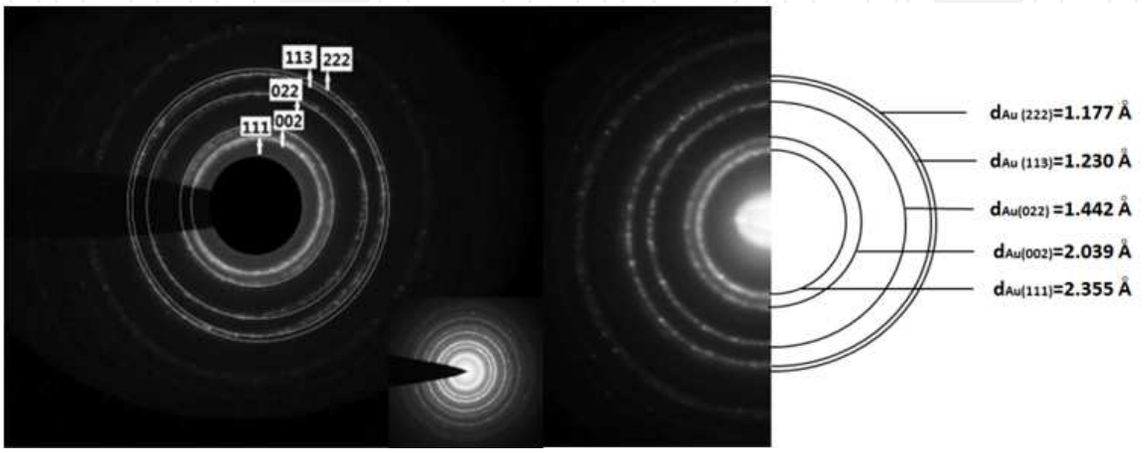

Figure 6. The ring diffraction pattern from a polycrystalline pure gold film with an f.c.c crystal structure. Crystal planes and interplanar spacing are shown by Miller indices. Camera lengths are 180 and 88 mm, respectively [4].

Analysis of ring patterns in polycrystalline materials (ultrafine grain) leads to identification of phases in materials. Diffraction patterns of nanoparticles produced by different methods form a ring pattern. In fact, the ring patterns are created when the nanoparticle is formed. Using the radius of each ring, we can specify the distance between the planes or interplanar spacing. Also, XRD analysis is used to determine the Miller indices for a set of planes. So, XRD analysis confirms the results of diffraction pattern from TEM for certain materials. A ring diffraction pattern from a polycrystalline gold specimen is shown in Figure 6. The interplanar spacing and lattice parameter can be calculated by measuring the radius of each diffraction ring (using Equation (10) and Table 2). Also, indexing ring patterns can be performed by XRD analysis [4–10].

2.1.1. Indexing ring patterns

In this chapter, an EM208S (Philips) transmission electron microscope operating at an accelerating voltage of 100 kV with a wavelength $\lambda = 3.7 \times 10^{-3}$ nm and camera length $L = 180,\ 88$ mm are used. One thing to note is that, accuracy and focus of TEM are very important to obtain an accurate diffraction pattern. Indexing methods used for ring diffraction patterns are as follows:

a. For known materials

1. Using the gold standard diffraction pattern, we define a scale on the picture of patterns to measure the radius diffraction pattern of specimens.

2. The first solution, with known lattice parameters, interplanar spacing is obtained from Equation (10) and Miller indices can be obtained using Table 2. The second solution, the ratio of outer ring to the first ring is equal to the reverse ratio of their interplanar spacing with possible Miller indices.

$$\frac{R_{outer}}{R_{first}} = \frac{d_{first}}{d_{outer}}$$

These possible Miller indices for planes are correct if the result of proportional relation above is almost the same.

b. For unknown material

1. Measure the radius of diffraction pattern like in the previous section.

2. Knowing the camera constant, interplanar spacing is obtained from Equation (10).

3. Compare interplanar spacing of unknown material with the ASTM index* to identify phases in diffraction patterns, Miller indices are determined for crystalline planes of phases in alloys [2, 6, 8].

*ASTM index to the powder diffraction file.

Crystal structure	Proportional relation for interplanar spacing	Possible values of algebraic relations Miller indices	Standard
Simple cubic	$\frac{1}{d^2} = \frac{h^2+k^2+l^2}{a^2} = \frac{N}{a^2}$	N an integer except 7 or 15	Proportional relation of squares of radius $\propto N$
f.c.c	$\frac{1}{d^2} = \frac{h^2+k^2+l^2}{a^2} = \frac{N}{a^2}$	N =3, 4, 8, 11, 12, 16, 19, 20	Proportional relation $\propto N$
b.c.c	$\frac{1}{d^2} = \frac{h^2+k^2+l^2}{a^2} = \frac{N}{a^2}$	N =2, 4, 6, 8, 10, 12, 14, 16, 18, 20	Proportional relation $\propto N$
Diamond structure	$\frac{1}{d^2} = \frac{h^2+k^2+l^2}{a^2} = \frac{N}{a^2}$	N =2, 8, 11, 16, 19	Proportional relation $\propto N$
Tetragonal	$\frac{1}{d^2} = \frac{h^2+k^2}{a^2} + \frac{l^2}{c^2}$	h^2+k^2=1, 2, 4, 5, 8, 9, 10, 13, 16, 17, 18, 20	Proportional relation often is 2
Hexagonal	$\frac{1}{d^2} = \frac{4}{3}\frac{h^2+hk+k^2}{a^2} + \frac{l^2}{c^2}$	h^2+hk+l^2=1, 3, 4, 7, 9, 12, 13, 16, 19	Proportional relation often is 3

Table 2. Proportional relations for interplanar spacing, Miller indices and lattice constant for different crystal structures [2]

2.2. Spot patterns

There are two basic parameters in spot diffraction patterns which are used to interpret and index such types of patterns. These parameters include

1. R is the distance between the diffracted and transmit (center spot) beams in the diffraction pattern screen. Also, this distance can be considered as a normal vector to the plane reflection.

2. The angles such as θ between two vectors drawn from the center to two adjacent points. In fact, each of these spots represents a set of planes, as can be seen in Figure 7.

The zone axis vector is parallel to the incident beam and is almost parallel with a set of reflected planes that is shown by $z=[uvw]$ with components u, v and w along the axis. The spots are in symmetry about the center of the pattern and, using the rules of vectors and the basic parallelogram, we can index spot patterns.

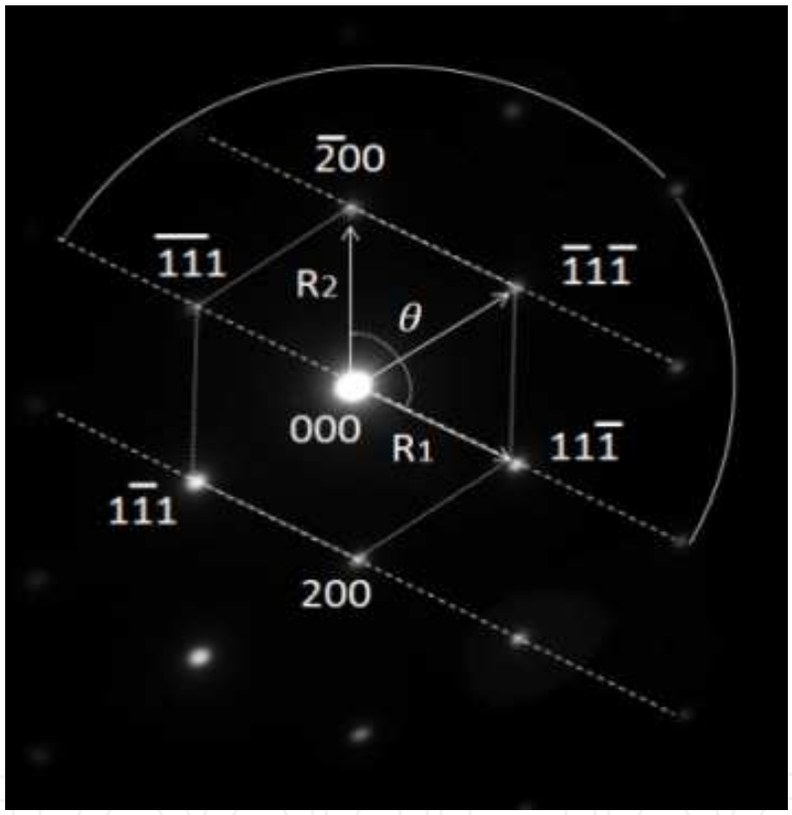

Figure 7. The spot diffraction pattern from a single crystal along zone axis $z=[011]$ of Al 1050 alloy with 10 passes of straight rolling.

2.2.1. Indexing spot patterns

For indexing spot patterns, indices of the spots and zone axis of single crystal materials should be determined. Here, we use the same indexing methods utilized for ring patterns as described in the previous section. In the experimental method, we measure distances of different spots from the center spot as well as angles on the micrograph of patterns and compare with patterns in the International Standard [17]. So, indices of spot and zone axis in pattern can be determined. The zone axis $z=[uvw]$ may be specified by the relations

$$\begin{aligned} u &= k_1 l_2 - k_2 l_1 \\ v &= l_1 h_2 - l_2 h_1 \\ w &= h_1 k_2 - h_2 k_1 \end{aligned} \tag{11}$$

where $h_1 k_1 l_1$ and $h_2 k_2 l_2$ are coordinates of each spot in the diffraction pattern [2, 5, 6, 8–12].

2.3. Kikuchi patterns

Kikuchi line pattern may happen when the thickness of the specimen is more than normal and almost perfect. These patterns occur by electrons scattered inelastically in small angles with a small loss of energy. Then, this beam of electrons is scattered elastically and creates Kikuchi lines in the patterns. Kikuchi lines in the pattern are pairs of parallel dark and bright lines. The distance between pairs of dark and bright lines is obtained by the following relation:

$$Dd_{hkl} = L\lambda \tag{12}$$

where D is the distance between pairs of Kikuchi lines. Also, the angle between Kikuchi lines in the pattern is in accordance with the angle between the diffraction planes because these lines are parallel with reflecting planes. The pairs of dark and bright lines, sets of reflecting planes and distance of paired lines are shown in Figure 8. The dashed lines are traces of the intersection of reflecting planes. By tilting the specimen, the Kikuchi line pattern changes by the displacement of paired lines. By increasing the sample thickness, the intensity of the spot pattern decreases and the intensity of Kikuchi line pattern increases. Most of the time, spot and Kikuchi line patterns exist simultaneously in micrographs, such as Figure 8. Basically, Kikuchi line patterns present more detailed information than the spot pattern. The appearance of explicit Kikuchi line patterns is a sign of crystal perfection.

2.3.1. Indexing Kikuchi line patterns

To study the crystal defects and to find out the orientation relationships, a tilting experiment should be used. The position of the Kikuchi line and spot patterns can be seen in Figure 9 in Al 7075 alloy in which a thermomechanical processing has been performed. To index the paired Kikuchi lines in the pattern, the distance between the pair of the Kikuchi lines may be measured. So, interplanar spacing can be determined using Equation (12). Consequently, a set of planes can be specified using the interplanar spacing and the type of material crystal structure.

3. Structural characterization of electron diffraction patterns

3.1. Orientation relationship

Relations between phases are determined by orientation relationships. Orientation relationships are indicated by a pair of parallel directions and a pair of parallel planes in two-phase

http://dx.doi.org/10.5772/61781

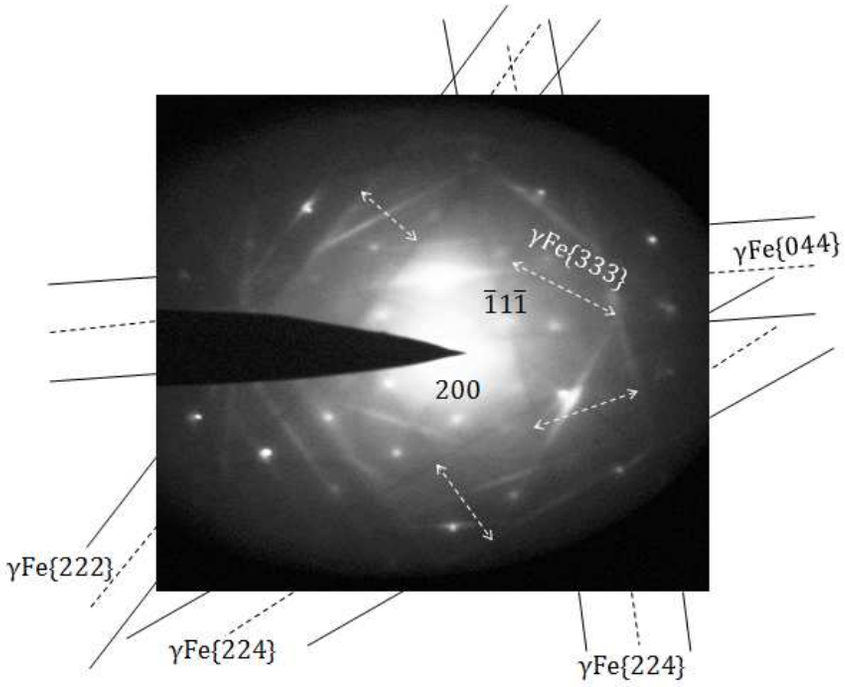

Figure 8. The spots, Kikuchi lines and the distance between paired Kikuchi lines in the pattern of γFe are determined.

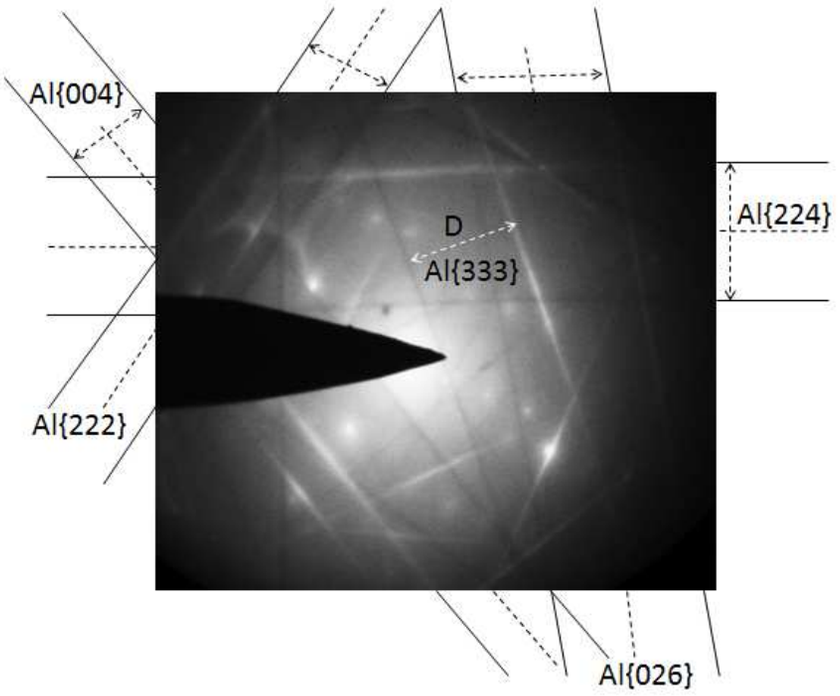

Figure 9. Spot and Kikuchi lines in the pattern of thermomechanically processed Al 7075 alloy. The distance between paired Kikuchi lines is presented as dark and bright lines.

materials. With the use of the spot pattern and Kikuchi line pattern methods, orientation relationships can be determined. Orientation relationships in two-phase alloys depend on

different factors such as types of crystal structural matrix, crystal structural precipitates, shape and size of precipitates. The spot diffraction pattern of quenched and tempered steel 0.1C-2.5V-2W-4.5Cr with chemical composition is illustrated in Figure 10a, which includes matrix spots (αFe) and precipitate spots (carbide$M_{23}C_6$). In the spot pattern of two-phase alloys, there exists two kinds of spots, as shown in Figure 10b. The precipitates and matrix are shown by small spots and big spots, respectively. Matrix has a b.c.c crystal structure and precipitates have a f.c.c crystal structure. So, the orientation relationship may be represented as

$$\left[\bar{1}11\right]_{\text{matrix}} // \left[\bar{1}11\right]_{\text{precipitate}}$$
$$\{011\}_{\text{matrix}} // \{022\}_{\text{precipitate}}$$

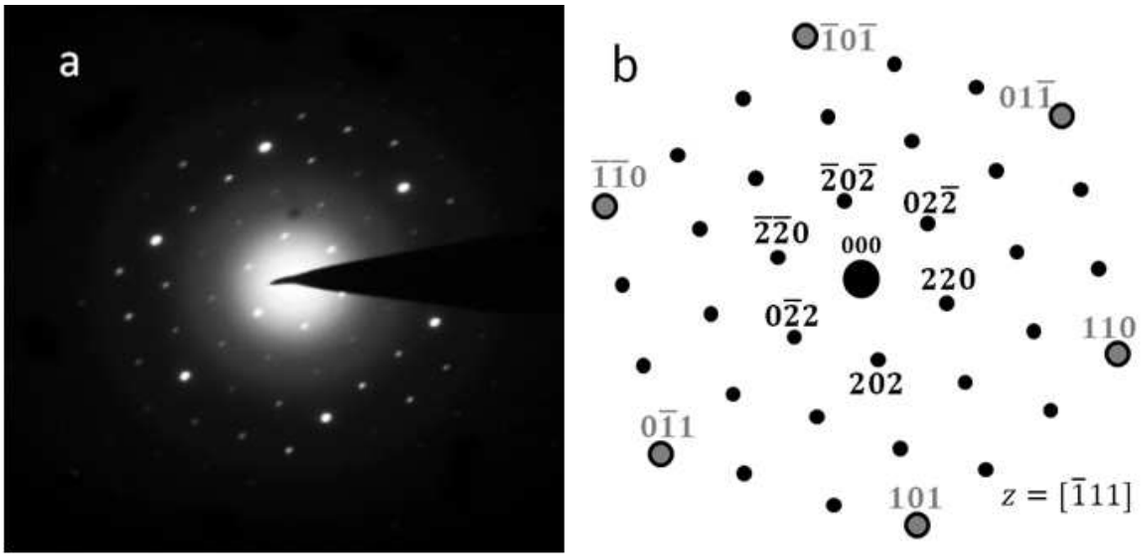

Figure 10. Spot diffraction pattern of quenched and tempered steel with 0.1C-2.5V-2W-4.5Cr composition that includes matrix spots (αFe) and precipitate spots ($carbide\ \ M_{23}C_6$). Small spots and big spots illustrate planes of matrix and planes of precipitate, respectively.

3.2. Phase identification

3.2.1. Phase identification in spot pattern

Interpretation and analysis of diffraction pattern is a method to identify the phases. These patterns can be composed of rings or spots. Generally, identification of phases using diffraction pattern is difficult, and other methods such as XRD should be used to verify the results. To identify the phases in a spot pattern, a spot diffraction pattern of Ti-6Al-4V alloy processed by forging is considered. This alloy contains α and β phases with c.p.h and b.c.c crystal structures, respectively. This pattern contains three different phases as shown in Figure 11. In this pattern, the bright and big spots are related to the α phase and the dim and small spots are related to the β phase.

http://dx.doi.org/10.5772/61781

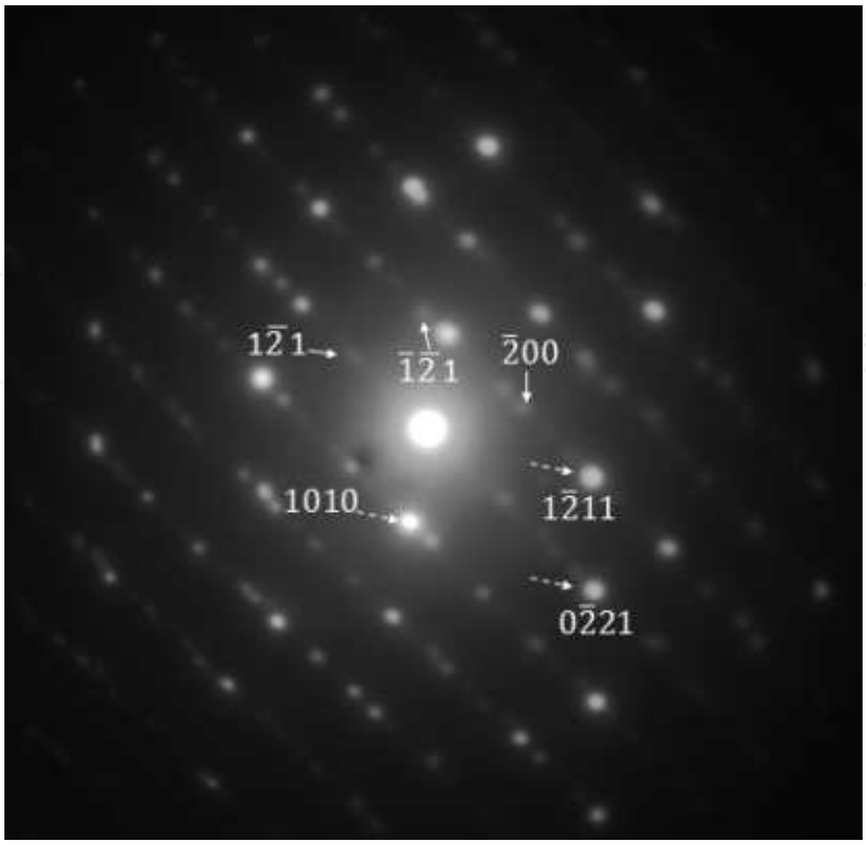

Figure 11. Spot diffraction pattern of forged $Ti-6Al-4V$ alloy. Two phases are observed in the pattern, namely, α and β with $Z=[\bar{1}2\bar{1}6]$ and $Z=[012]$, respectively.

3.2.2. Phase identification in the ring pattern

Carbon nanotubes (CNTs) added to a metal matrix can exhibit significant properties. The main challenge in CNTs-reinforced composites is the uniform dispersion of CNTs in the matrix. Several methods such as ball milling have been developed for distribution of the CNTs in metal matrices. For example, a milled sample of 20 wt% multi-wall carbon nanotubes (MWCNT) + Al powder was investigated using the EDP method. In addition, their corresponding EDP is shown in Figure 12a. To separate ring patterns of CNTs and aluminum, a ring pattern of Al was attached to the EDP of Al-CNTs composite, as illustrated in Figure 12b. This technique helps to better identify the two phases [7].

3.3. Twinning

Twinning is one of the crystalline defects that appear mainly as two parallel planes. Additional spots are created around the main spots of diffracted planes in the pattern by twinning because orientation of twinning is different from the crystal lattice. The direction of the reflected planes inside the twinning is not the same as the whole crystal structure and extra spots become visible in the diffraction pattern.

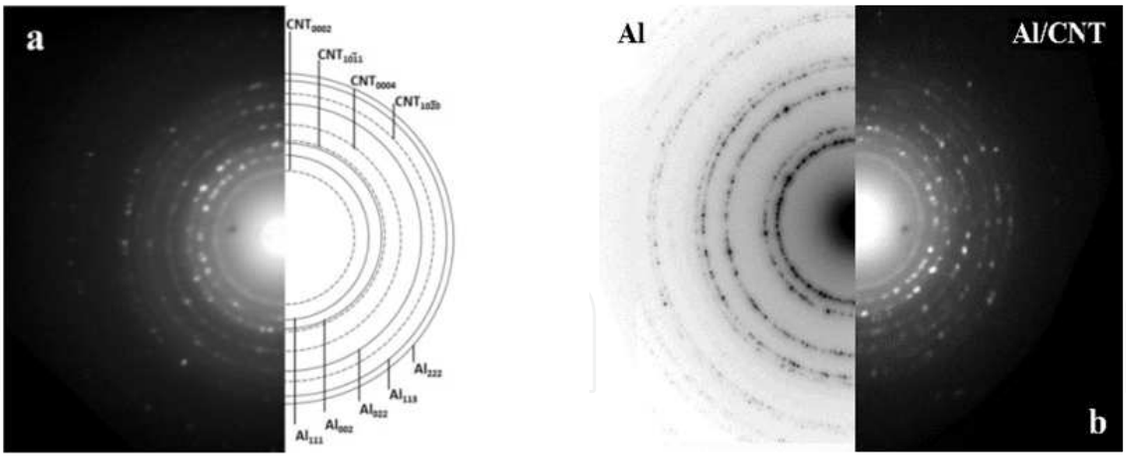

Figure 12. The SAED patterns of CNT-reinforced Al powders, (a) planes of Al and CNT are determined and indexed (b) Al/CNT and Al patterns are in a single pattern to identify phases.

For indexing a twining spot pattern in a cubic crystal structure

1. The main spots of the material are identified and indexed in accordance with the previous section.

2. Twinning spots are determined and indexed by 180° rotation around the {111} and {112} planes for f.c.c and b.c.c crystal lattices, respectively.

Basically, f.c.c crystal structure twins on {111} planes and b.c.c crystal structure on {112}. Twin spots in γFe pattern with a f.c.c crystal lattice are indexed according to Figure 13. The spot diffraction pattern of matrix and twin are mirror reflections across the $(1\bar{1}1)$ plane.

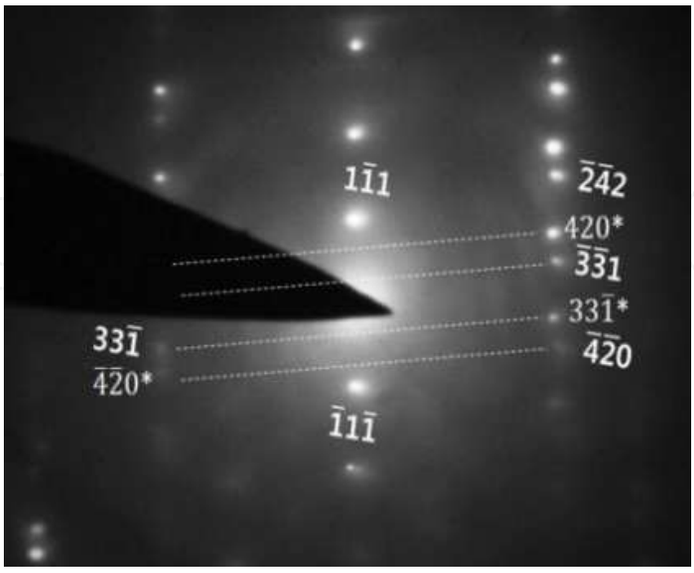

Figure 13. Twinning spots pattern from γFe with f.c.c crystal lattice which index matrix and twin spots with zone axis $z=[\bar{1}23]$, twinned on $(1\bar{1}1)$, hkl* planes related to twin planes and hkl planes related to main reflected planes.

3.4. Dislocation

The equal channel angular pressing (ECAP) and cryo-cross-rolling process have been performed on Al 5083 alloy and Al 1050 alloy with two passes and ten passes, respectively. These processes create a high dislocation density in Al matrix, which affects the shapes of spots in the diffraction pattern. Also, the diffraction patterns of these alloys illustrate streaks on spots due to high accumulation of dislocations and many partial rings due to preferred orientation. Spots in the pattern deform from a usual shape (circular shape) to stretched and irregular spots (disk-type halo). Dislocations change the crystal orientation locally and diffraction spots are extended along the diffraction ring as seen in Figure 14a,b.

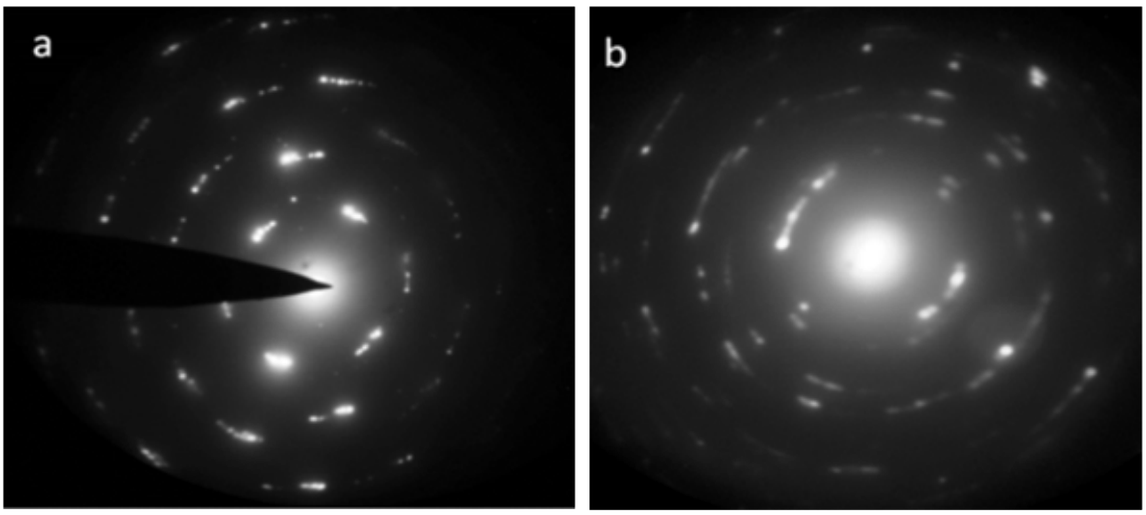

Figure 14. (a) Diffraction pattern of Al 5083 alloy with two passes of equal channel angular pressing and (b) diffraction pattern of Al 1050 alloy with ten passes of cryo-cross-rolling process illustrate streaks on spots due to high density of dislocations.

3.5. Preferred orientation and texture

In certain specimens, preferred orientation of planes occur by some mechanical processes such as various types of rolling and ECAP. If the crystal structure in the specimen is oriented in a favored and preferred direction, the SAED pattern will be formed from many partial rings, as shown in Figure 15. Diffraction pattern obtained from the texture can be considered as an intermediate case between the diffraction from a single crystal and a polycrystalline material. The texture created in alloys may be investigated by interpretation of their diffraction patterns. The preferred orientation {110} [001] is created in Al 2024 alloy by ECAP process.

3.6. Streaks

Presence of fine structure such as streaks and extra spots in many patterns is an indication of the presence of crystal defects which include dislocations, different types of precipitates, twins and staking faults. So, the type of streaks arising in patterns depends on several factors such as various structural defects in the lattice, specimen conditions and diffraction conditions. The

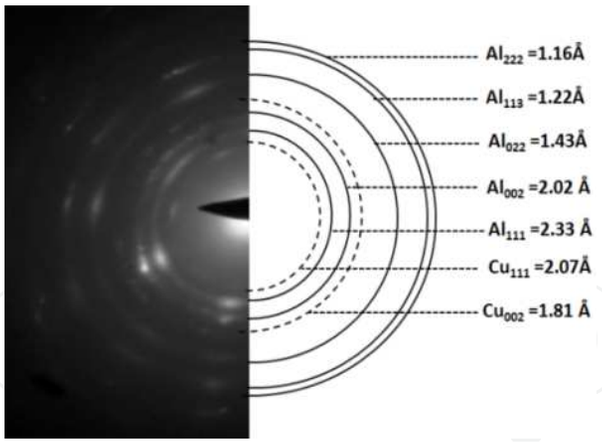

Figure 15. The diffraction pattern for Al 2024 alloy with 4 passes of ECAP, showing the preferred orientation of specimen.

main factors in streaks are precipitates, stacking faults, twins and dislocations. Different shapes of precipitate determine the shapes of reciprocal lattice. So, the final shape of spot patterns depends on the types of precipitates. Streaks on spot pattern are created by stacking faults of quasi-sphere and rod particles of carbide M_7C_3, as shown in Figure 16a. The corresponding spot diffraction pattern illustrates long streaks (diffuse scattering). In fact, streaks in the diffraction pattern can be created by stacking faults in any crystal structure. Depending on the diffraction conditions, streaks or enlarged spots and extra spots or pseudo-satellites will be created, as shown in Figure 16b.

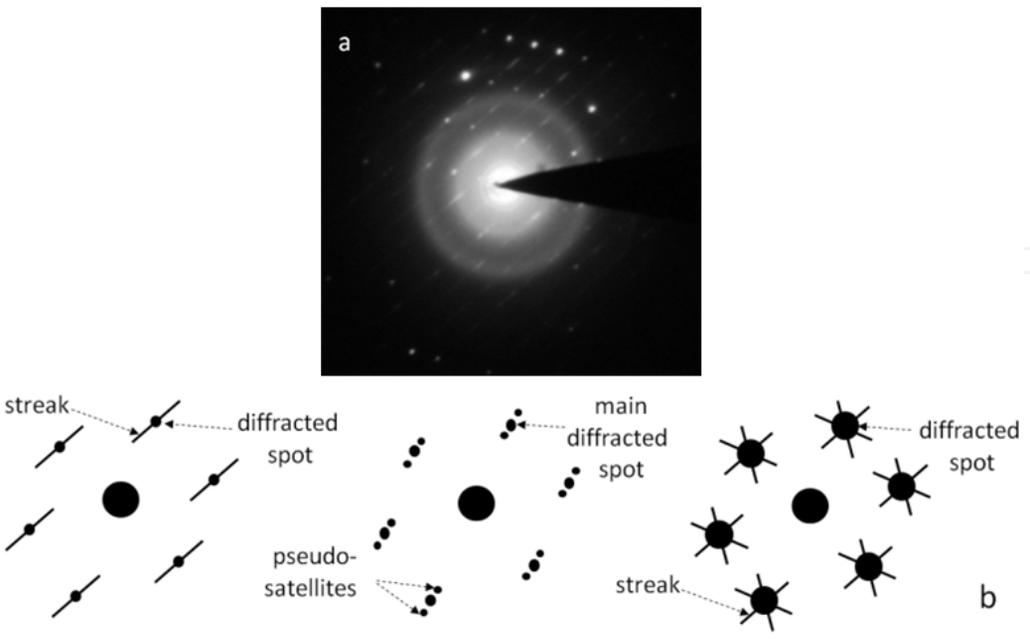

Figure 16. (a) Streaks on spots due to stacking faults of carbide M_7C_3 quasi-sphere and rod particles are created, (b) different types of streaks in the spot diffraction pattern in various conditions of diffraction.

http://dx.doi.org/10.5772/61781

4. Electron diffraction pattern of new materials

4.1. Highly crystalline Multi-Wall carbon Nanotubes (MWNTs)

It should be noted that the structure of CNTs depends substantially on the synthesis methods. A ring pattern of the sample demonstrates a crystal structure corresponding to a graphite ring pattern. As a result, the interplanar spacing of MWCNTs is almost similar to the interplanar spacing of graphite. Thus, the interplanar spacing of nanotubes is indexed using the graphite crystal structure as shown in Figure 17a. With this interpretation, crystal structure of MWCNTs is hexagonal and its lattice parameters are a=2.41 $\mathring{A}$ and c=6.61$\mathring{A}$. In MWCNTs, many amorphous carbons exist as impurities which are created during the production process. Also, the CNTs are complicated and in the shape of a coil. For this reason, the shape of their EDP is a coaxial ring as well as the halo shown in Figure 17b. The EDP of MWCNTs have many rings, each one corresponds to a set of atomic planes. Highly crystalline MWCNTs are a type of MWCNTs with identical chiralities of zigzag type that do not have any impurity and are constructed from monochirality graphite shells. These kinds of CNTs are synthesized by a low-temperature chemical vapor deposition process in plasma. The EDP of highly crystalline MWCNT made of two simple hexagonal patterns overlapping each other is seen in Figure 17b. It is noteworthy that the EDP is taken from an area on the wall of the nanotube. Their spot pattern shows that all of the layers have almost the same chirality.

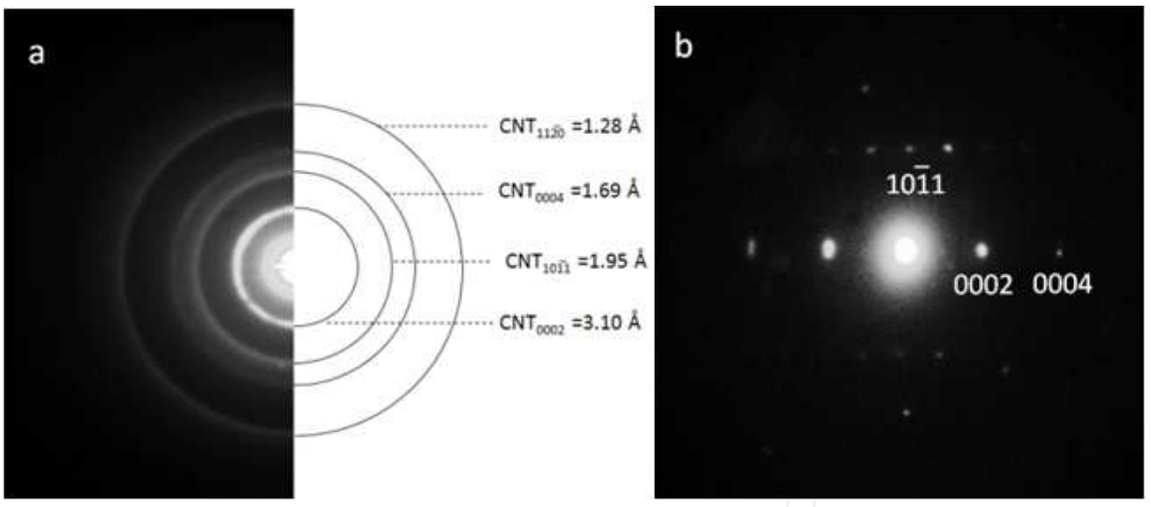

Figure 17. (a) The ring diffraction pattern of coiled MWCNT, (b) the spot diffraction pattern of highly crystalline MWCNT.

4.2. Palladium doping into MWCNTs

Various methods are available for doping nanoparticles into CNTs which give specific features to them and changes the optical, transport, magnetic, electronic and chemical properties of CNTs. In this investigation, a couple of Pd nanoparticles doped into MWCNTs by chemical methods are selected. The EDP of the selected area on the sample is shown in Figure 18. The

ring and spot patterns belong to CNTs and palladium nanoparticles, respectively. Atomic planes can be determined by measuring distances and angles between spots. According to the results of measurements, palladium has a f.c.c crystal structure and the lattice parameter and zone axis of the sample are 3.90 $\mathring{A}$ and z=[$\bar{1}$22], respectively.

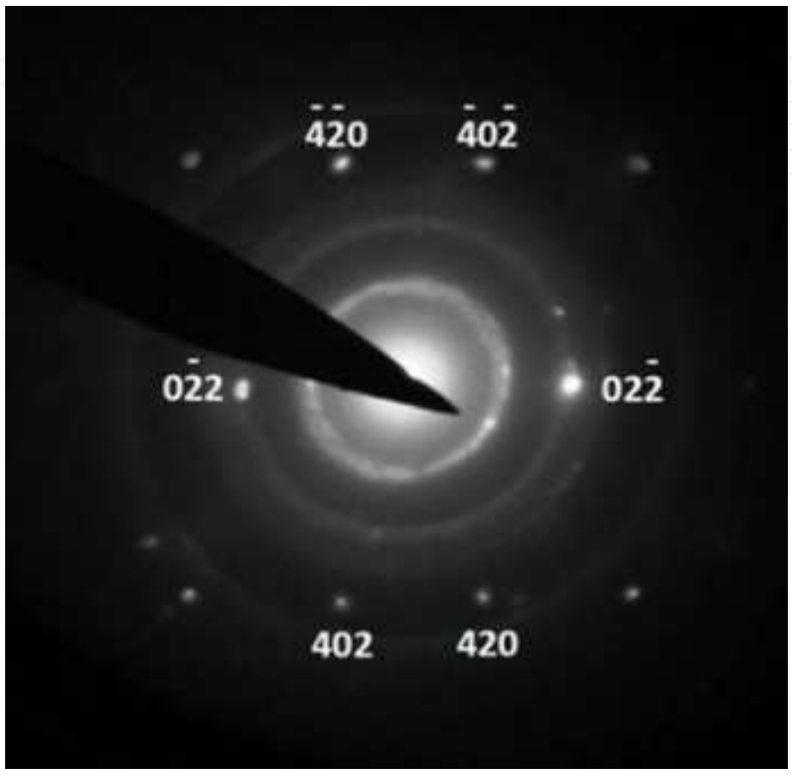

Figure 18. The ring pattern of MWCNTs superimposed on the spot patterns of palladium.

4.3. Vanadium Oxide Nanotubes (VONTs)

In order to study the organic nanotubes, VONTs were selected. It is noteworthy that using EDP method and its interpretation results, structure of various nanotubes will be predictable. Figure 19 shows a ring diffraction pattern of VONTs. Interplanar spacing and lattice parameter can be determined by analysing the ring diffraction pattern. The ring pattern with the Miller indices according to the interplanar spacing of VONTs crystal structure is given. Based on the results of the measurements, VONT has a f.c.c crystal structure and its lattice parameter was 3.92 $\mathring{A}$. In addition, the results of EDP technique have been approved by XRD analysis.

4.4. Amorphous coating

When the grain size of the specimen is extremely fine or completely amorphous, the feature of concentric rings in the pattern disappears and a halo is left around the bright center spot, which shows that the electrons are scattered randomly by the amorphous structure of specimen. The amorphous and glassy materials are identified by this method. Diffraction

http://dx.doi.org/10.5772/61781

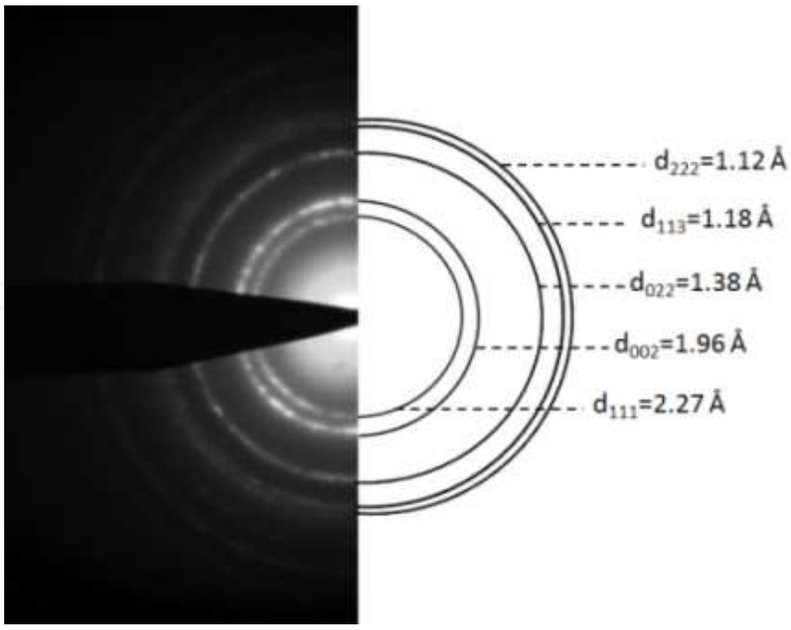

Figure 19. The ring diffraction pattern of VONT, interplanar spacing and planes are determined.

pattern for amorphous coating of silica-zinc oxide multilayered nano-porous membrane on α-alumina substrate prepared by sol-gel method is shown in Figure 20.

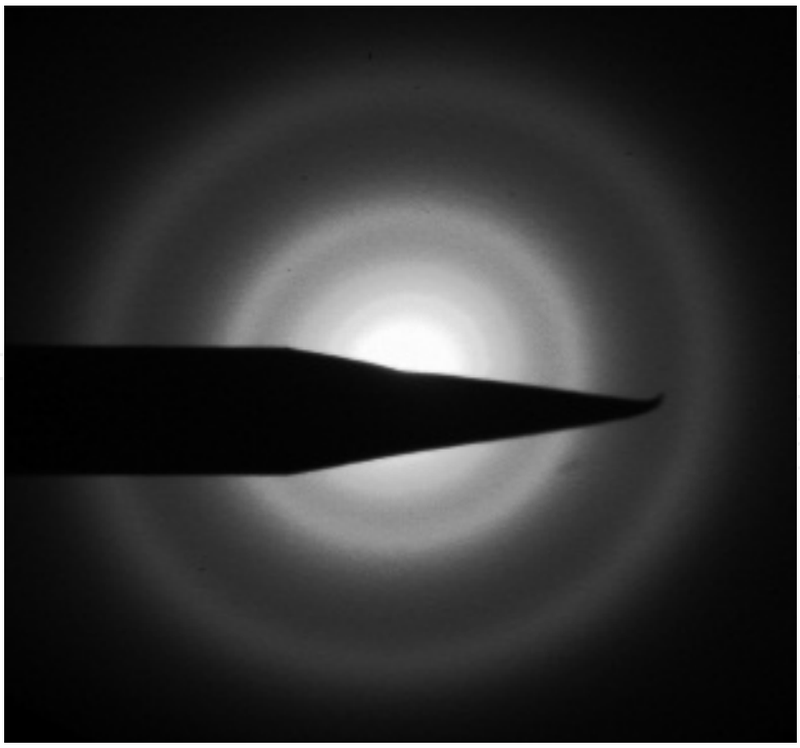

Figure 20. The diffraction pattern of amorphous coating $SiO_2-10\%$ ZnO prepared with sol-gel method on α-alumina substrate.

5. Appendix 1

Accelerating voltages (kV)	λ (Å)
50	0.0536
100	0.0370
200	0.0251
500	0.0142
1000	0.0087

Table 3. Electron wavelength λ for applied accelerating voltages in electron microscopy

Author details

Mohsen Asadi Asadabad* and Mohammad Jafari Eskandari

*Address all correspondence to: asadimohsen@gmail.com

Materials Research School, NSTRI, Isfahan, Iran

References

[1] Cowley J M. Diffraction Physics, third revised edition, Elsevier; 1995. DOI:10.1016/B978-0-444-82218-5.50024-9.

[2] Edindton J W. Electron Diffraction in the Electron Microscope. London, Macmillan; 1975.

[3] K. W. Andrews. Interpretation of Electron Diffraction Patterns. London, ADAM HILGER LTD, 1971.

[4] Asadi Asadabad M, Jafari Eskandari M. Transmission electron microscopy as best technique for characterization in nanotechnology. Synthesis and Reactivity in Inorganic, Journal of Metal-Organic, and Nano-Metal Chemistry. 2015; 45, 323–326. DOI: 10.1080/15533174.2013.831901.

[5] Weirich T E, Lábár J L, Zou X. Electron crystallography. Novel Approaches for Structure Determination of Nanosized Materials. Springer; 2004.

[6] Beeston B E P, Horne R W, and Markham R. Electron Diffraction and Optical Methods in Electron Diffraction Techniques. Elsevier, North Holland. 1972.

[7] Asadi Asadabad M, Jafari Eskandari M, Tafrishi R, Emamalizadeh M. Transmission electron microscopy characterization of diffraction nanotubes, Submitted.

[8] Hammond C. The Basic of Crystallography and Diffraction. Oxford, Oxford Science Publications; 1997.

[9] M. Jafari Eskandari, R. Tafrishi, M. Asadi Asadabad. Study of the nanostructure evolution in aluminum 1050 sheet by cryo-cross-rolling process, Submitted.

[10] Hirsch P B, Howie A, Nicholson R B, Pashley D W, and Whelan M. Electron Microscopy of Thin Crystals, London, Butterworth; 1965.

[11] Hren J J, Goldstein J I, and Joy D C. Introduction to Analytical Electron Microscopy. Plenum; 1979.

[12] Ball C J. An Introduction to the Theory of Diffraction. Pergamon, Oxford; 1971.

[13] Rymer T B, Electron Diffraction, Methuen, London; 1970.

[14] Vainshtien B K, Structure Analysis by Electron Diffraction. Pergamon Press, Oxford; 1964.

[15] Asadi Asadabad M, Jafari Eskandari M, Tafrishi R, Bagherzadeh M. The effect of cross-rolling process on nanostructure of Al 1050 alloy. Journal of Nanoanalysis. 2014; 1: 93–98.

[16] Microbeam analysis, analytical electron microscopy, selected-area electron diffraction analysis using a transmission electron microscope, International Standard, ISO 25498, First edition, 2010.

[17] David B, Williams C. Barry Carter. Transmission electron microscopy. A Textbook for Materials Science. Springer Science Business Media; LLC 1996, 2009.

[18] Mogilevsky P, et al., Evolution of texture in rhabdophane-derived monazite coatings. Journal of the American Ceramic Society. 2003; 86: 1767–1772. DOI: 10.1111/j. 1151-2916.2003.tb03552.

[19] Fillingham P J, Leamy H J, and Tanner L E. Electron Microscopy and Structure of Materials, University of California Press; 1972.

[20] Hollox G E, Rowcliffe D J, and Edington J W, Electron Microscopy and Structure of Materials. University of California Press; 1972.

[21] Thomas G, Modern Diffraction and Imaging Techniques in Materials Science. North-Holland; 1970.

IntechOpen